# Aspartic Acid Residue D3 Critically Determines Cx50 Gap Junction Channel Transjunctional Voltage-Dependent Gating and Unitary Conductance

Li Xin,[†] So Nakagawa,[‡] Tomitake Tsukihara,[‡] and Donglin Bai[†*]

[†]Graduate Program of Neuroscience, Department of Physiology and Pharmacology, University of Western Ontario, London, Ontario, Canada; and [‡]Institutes for Protein Research, Osaka University, Osaka, Japan

ABSTRACT Previous studies have suggested that the aspartic acid residue (D) at the third position is critical in determining the voltage polarity of fast $V_j$-gating of Cx50 channels. To test whether another negatively charged residue (a glutamic acid residue, E) could fulfill the role of the D3 residue, we generated the mutant Cx50D3E. $V_j$-dependent gating properties of this mutant channel were characterized by double-patch-clamp recordings in N2A cells. Macroscopically, the D3E substitution reduced the residual conductance ($G_{min}$) to near zero and outwardly shifted the half-inactivation voltage ($V_0$), which is a result of both a reduced aggregate gating charge ($z$) and a reduced free-energy difference between the open and closed states. Single Cx50D3E gap junction channels showed reduced unitary conductance ($\gamma_j$) of the main open state, reduced open dwell time at $\pm 40$ mV, and absence of a long-lived substate. In contrast, a G8E substitution tested to compare the effects of the E residue at the third and eighth positions did not modify the $V_j$-dependent gating profile or $\gamma_j$. In summary, this study is the first that we know of to suggest that the D3 residue plays an essential role, in addition to serving as a negative-charge provider, as a critical determinant of the $V_j$-dependent gating sensitivity, open-closed stability, and unitary conductance of Cx50 gap junction channels.

## INTRODUCTION

Gap junction (GJ) channels connect neighboring cells in vertebrates and invertebrates, and allow for ions and small molecules to pass between cells. These channels exhibit a property whereby their aggregate junctional conductance ($G_j$) is regulated by transjunctional voltage ($V_j$), which is the voltage difference between the interiors of the cells that the channels connect. GJ channels composed of different connexin (Cx) subunits show varying degrees of sensitivity to $V_j$, gating polarities (positive or negative), and kinetic properties (1,2). As initially reported in the junctions of amphibian blastomeres (3,4), the $G_j$ of most junctions composed of a single type of Cx is typically maximal at $V_j = 0$ ($G_{max}$), and decreases symmetrically for positive and negative $V_j$ pulses to a nonzero residual conductance. The steady-state $G_j/V_j$ curves can be well approximated by a two-state Boltzmann function at each $V_j$ polarity (3) and parameterized by minimum residual conductance ($G_{min}$), half inactivation voltage ($V_0$), and the steepness of the curve ($A$). $V_j$ sensitivity is reflected by the parameter $A$ in terms of the apparent gating charge ($z$) involved in voltage sensing. GJ channels composed of different types of Cx subunits show divergent Boltzmann parameters. For instance, the magnitude of $G_{min}$ ranges from ~5% (e.g., Cx45 channels) to values of up to ~60–80% (e.g., Cx36 or hCx31.9 and orthologs); the apparent gating charge ranges from $z = 11.3$ (e.g., mCx37) to $z = 1.3$ (e.g., mCx36), and $V_0$ from ~10 mV (e.g., chCx45) to above 100 mV (e.g., mCx36) (5–11).

Many structural and functional studies have focused on identifying the molecular mechanism underlying $V_j$-dependent gating properties. A recently reported high-resolution crystal structure of the human Cx26 GJ channel provided a structural basis for the presence of the amino terminus (NT) in the gap junction pore, thereby allowing it to sense changes in the electrical field within the pore. Moreover, Cx26 and Cx32 were the first Cxs utilized for elucidating the functional importance of the NT in $V_j$-dependent gating (12). Mutational analyses revealed that the presence of a negatively charged aspartic acid residue (D) at the second position was correlated with the positive polarity of $V_j$-induced closure of the Cx26 GJ channel. More recently, a mutation of the corresponding residue in Cx50 (Cx50D3N) showed changes in $V_j$-dependent gating that were thought to result from either disrupted gating or a reversal of gating polarity from positive to negative (13,14). However, whether the role of D3 in determining $V_j$-dependent gating can be fulfilled by another negatively charged residue, glutamic acid (E), whose side chain is only one methylene group (-CH2-) longer than that of D, has yet to be tested. Given the fact that the residue E also exists in the third position of other Cxs, such as Cx36 and hCx31.9, it is of great interest to know whether these two residues (D and E) are critical to the transduction of $V_j$-dependent gating in Cx50 and Cx36, respectively.

Previous work has shown that a chimera, Cx50-Cx36N, in which the NT of Cx50 was replaced by that of Cx36, exhibited modified $V_j$-dependent gating properties and

*Submitted July 4, 2011, and accepted for publication February 8, 2012.*

*Correspondence: donglin.bai@schulich.uwo.ca

Editor: Tzyh-Chang Hwang.



0006-3495/12/03/1022/10 $2.00

doi: 10.1016/j.bpj.2012.02.008

reduced unitary conductance ($\gamma_j$) (15). Further characterization of a mutant (Cx50N9R, in which the Asn (N) at position 9 is replaced by Arg (R)) demonstrated that the positively charged R substitution at the ninth position of the Cx50 NT resulted in near-zero $G_{min}$ values and ~20-mV outward shifts of $V_0$, coupled with an ~50% reduction of $z$. However, how the two negatively charged residues (E3 and E8) native to Cx36 (Fig.1 *A*) would affect Cx50 GJ channel properties has yet to be examined.

Accordingly, here we examined three mutants, Cx50D3E, Cx50G8E, and Cx50GNI (the last being a triple mutation composed of G8E, N9R, and I10L substitutions) and characterized their $V_j$-dependent gating and $\gamma_j$ by performing double patch-clamp recordings in neuroblastoma (N2A) cells. Macroscopically, the Cx50D3E channels displayed apparent changes in the $V_j$-dependent gating profile; microscopically, they showed a reduced $\gamma_j$ and absence of long-lived substate. By contrast, Cx50G8E and Cx50GNI mutants slightly shifted the $V_0$ without changing the apparent gating charge, whereas single-channel main $\gamma_j$ and subconductance level were indistinguishable from those of the wild-type Cx50 GJ channels. Our data suggest that the negatively charged residue D at the third position critically determines the $V_j$-gating sensitivity, the balance of open-closed state stability, and unitary conductance of Cx50 GJ channels, whereas mutations at positions 8, 9, and 10 do not affect the $V_j$-dependent gating sensitivity.

## MATERIALS AND METHODS

### Generation of cDNA constructs: Cx50D3E, Cx50G8E, and Cx50GNI

The three mutants assessed in this study are highlighted on the primary sequence alignment of NT between mouse Cx50 and Cx36 (Fig. 1). Mutant cDNAs were generated by using the site-directed mutagenesis approach. The primers used to generate Cx50D3E (mutation of aspartic acid residue to glutamic acid residue), forward 5′-3′: TCTGCAGAATTCATGGGCGA GTGGAGTTTCCTGGGAAAC, reverse 5′-3′: GTTTCCCAGGAAACT CCACTCGCCCATGAATTCTGCAGA; Cx50G8E (mutation of glysine (G) residue to E residue), forward 5′-3′: GGAGTTTCCTGGAAAAC ATCTTGG, reverse 5′-3′: TCCAAGATGTTTTCCAGGAAACTCC; Cx50GNI (including three mutations: G to E, N to R, and isoleucine (I) to leucine (L)), forward 5′-3′: GGCGACTGGAGTTTCCTGGAAAGACT CTTGGAAGAGGTGAATGAGCAC, reverse 5′-3′: GTGCTCATTCACCT CTTCCAAGAGTCTTTCCAGGAAACTCCAGTCGCC. All the mutant cDNAs were cloned into the pcDNA3.1-vector, with plasmids purified using a Plasmid Maxi Kit (Qiagen, Valencia, CA) and mutation confirmed by sequencing.

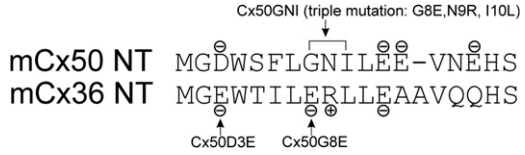


FIGURE 1 Mutants examined in this study. NT primary sequence alignment between mouse Cx36 and Cx50 shows the positions of mutants. Negatively and positively charged residues are labeled – and +, respectively. In Cx50D3E, D was replaced by E at the third position, and in Cx50G8E, G was replaced by E at the eighth position; Cx50GNI is a triple mutation, in which G, N, and I were replaced by E, R, and L, respectively.

### N2A cell culture, transfection, and Immunolabeling

HeLa cells and mouse neuroblastoma (N2A) cells were purchased from ATCC (American Type Culture Collection, Manassas, VA) and grown in Dulbecco's modified Eagle's medium containing high glucose with 2 mM L-glutamine, no sodium pyruvate, supplemented with 10% fetal bovine serum, 100 $\mu$M penicillin, and 100 $\mu$g/ml streptomycin sulfate, in a humidified atmosphere of 5% $CO_2$ at 37°C. Transient transfections were performed on N2A cells grown to 80–90% confluence in a 35-mm petri dish using Lipofectamine 2000 (Invitrogen, Carlsbad, CA) as described previously (16). Immunolabeling was performed by using the primary antibody, polyclonal goat-antiCx50 (K20, Santa Cruz, CA), which is recognized by Alexa-488 conjugated anti-goat IgG (Invitrogen). Fluorescent images were acquired as described previously (16).

### Electrophysiological recordings

N2A cells were replated on 1-cm-diameter glass coverslips 24–48 h after transfection. Coverslips were transferred to a recording chamber on the stage of an inverted microscope (DM IRB, Leica, Wetzlar, Germany) 1–3 h after replating and bathed in an external solution (15,17). Double whole-cell patch clamp recordings were performed using two Axopatch 200B amplifiers (Axon Instruments, Union City, CA). Voltage-step protocols (see Fig. 3 *A*) were applied to characterize the transjunctional voltage-dependent gating and single-channel properties. All macroscopic signals were digitized at 10 kHz and filtered at 1 kHz. Macroscopic junctional conductance ($G_j$) was calculated by dividing the measured junctional current by the transjunctional voltage: $G_j = I_j/V_j$. To ensure accuracy, off-line compensation was used to correct junctional voltage errors resulting from the series resistance, $R_{el}$, of each patch electrode in the $G_j$ calculations according to the expression (18)

$$G_j = -\frac{\Delta I_2}{[V_1 - (I_1 R_{ell}) - V_2 + (I_2 R_{e12})]}$$

Only those cell pairs with a $G_j$ of <9 nS were chosen to study $V_j$-dependent gating, to minimize the errors of series resistance on these measurements (19,20). The peak level of junctional current was measured at the beginning of the trace, whereas the steady-state level was measured by taking the average junctional current of the last 500 ms of each trace. Steady-state junctional currents at each voltage step were normalized relative to the peak currents, and these normalized $G_{j,ss}$ values were plotted as a function of the $V_j$. The relationship between $G_{j,ss}$ and $V_j$ was then fitted with a two-state Boltzmann equation (3,21),

$$G_{j,ss} = \frac{(G_{max} - G_{min})}{\{(1 + \exp[A(V_j - V_0)]\}} + G_{min},$$

where $G_{max}$ is the theoretical maximum conductance extrapolated from the experimental data; $G_{min}$ is the extrapolated value of residual conductance; $V_0$ is the half-inaction voltage at which $G_{j,ss} = (G_{max} + G_{min})/2$ and $A = zq/KT$ reflects the voltage sensitivity in terms of the number of equivalent gating charges, $z$, moving through the entire applied field, where $q$ is the electron charge and $K$ and $T$ are the Boltzmann constant and absolute temperature, respectively.

Recordings from only cell pairs displaying one or two channels were used to determine the unitary current amplitudes. The unitary conductance

($\gamma_j$) was calculated by dividing the measured amplitudes of single-channel current ($I_j$) by the $V_j$; $\gamma_j = I_j/V_j$. The amplitudes were determined either by direct measurement of the traces or by first plotting all-points amplitude histograms and then fitting these histograms with Gaussian functions to determine the mean and variance of the baseline and open channel current (22). The current signal was filtered at 1 kHz and digitized at 10 kHz, and the recorded unitary current was digitally filtered by a low-pass Gaussian filter (200 Hz) for presentation. The current traces recorded at ±40 mV were digitally filtered at 500 Hz for the analysis of the dwell time of the main open state. Close times <2 ms were eliminated from analysis, as this is beyond the resolution of our single-channel records. The mean open dwell time was determined by constructing the logarithmic histograms (10 bins/decade) of dwell time and fitting them to an exponential function (23).

Macroscopic and single-channel data were acquired using a PC computer through a Digidata 1322A AD-DA interface and pClamp 9.0 software (Axon Instruments). Groups statistics are expressed as mean ± SE. One-way ANOVA were used to compare groups of data for statistical difference.

## RESULTS

### Cx50D3E, Cx50G8E, and Cx50GNI are all capable of trafficking to the cell surface

To characterize the cellular localization of Cx50 mutants (D3E, G8E, and GNI), we utilized gap-junction-deficient HeLa cells to transiently overexpress these constructs. Similar to their wild-type counterpart, all three mutants were able to traffic to the cell membrane and cell-cell interfaces (Fig. 2, *arrows*), although in some cases the Cx was also found at locations other than cell-cell interfaces in the plasma membrane, and at cytosolic locations. The ability of the Cx50 mutants to traffic to the cell surface is essential for the formation of functional GJ channels. Similar results were also observed in N2A cells (data not shown).

### Cx50D3E exhibits novel $V_j$-dependent gating properties compared to Cx50

The $V_j$-dependent gating properties of the Cx50D3E GJ channel were determined by transiently expressing this mutant in N2A cells and conducting dual whole-cell patch-clamp recordings. For this purpose, a pair of cells was initially held at a common holding potential of 0 mV, and thereafter, one cell of the pair underwent a series of positive and negative voltage steps (each 7 s in duration) between −100 mV and +100 mV in 20-mV increments to establish a $V_j$ gradient while the $I_j$s were measured at the other cell (Fig. 3 *A*). The interval between steps was 30 s. A representative family of $I_j$ is illustrated in Fig. 3 *B*. The amplitude of $I_j$ declined at voltage steps of ±20 mV, with continual symmetrical reduction to steady-state levels at both voltage polarities, and to greater degrees with increasing voltages. The steady-state $G_j$ values were normalized to their corresponding peak $G_j$ at $V_j = 0$ mV to obtain $G_{j,ss}$ and plotted against $V_j$. For each polarity, the relationship of $G_{j,ss}/V_j$ was well fit by a single two-state Boltzmann equation and was characterized by an equivalent gating charge ($z$) of 1.1 ± 0.4, $V_0$ of 45.1 ± 5.4 mV, and $G_{min}$ of 0.02 ± 0.01 for the negative $V_j$, and a $z$ of 1.3 ± 0.3, $V_0$ of 43.3 ± 3.9 mV, and $G_{min}$ of 0.07 ± 0.06 for the positive $V_j$. From the measured Boltzmann parameters, $z$ and $V_0$, we calculated the free-energy difference ($\Delta G_0$) between the aggregate open and closed states in the absence of a field according to the equation $\Delta G_0 = zFV_0$ (24,25). The $\Delta G_0$ of D3E channels (4.9 ± 1.8 and 5.5 ± 1.4 kJ mol$^{-1}$ for negative and positive $V_j$, respectively) were significantly reduced ($p < 0.05$) compared to those of wild-type Cx50 (14.6 ± 3.9 and 15.3 ± 4.0 kJ mol$^{-1}$). The $G_{j,ss}/V_j$ curve of Cx50 documented in our previous study (15) is superimposed on that of Cx50D3E for visual comparison (Fig. 3 *C*), and the Boltzmann parameters and the $\Delta G_0$ values are listed in Table 1. These results demonstrate that the D3E substitution reduces the $V_j$-dependent gating sensitivity of Cx50 channels by reducing the apparent gating charge by ~70%. In addition, it reduces the energy difference between the aggregate open and closed states. The combined effects of these changes are to decrease occupancy of the open state at $V_j = 0$ relative to wild-type (due to reduced $\Delta G_0$), but to increase open-state occupancy with increasing $V_j$ (e.g., at ±60 mV) relative to wild-type (due to decreased $z$).

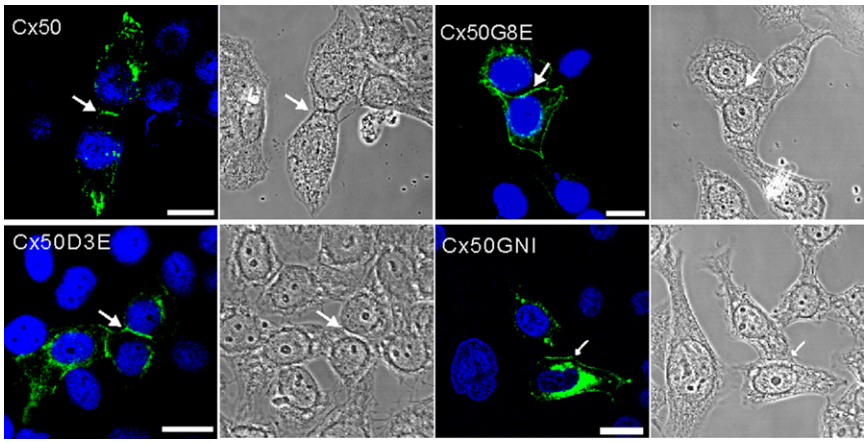


FIGURE 2 Immunolabeling of mutant proteins in HeLa cells. All three mutants shown here (Cx50D3E, Cx50G8E, and Cx50GNI) were able to reach the cell surface and cell-cell interfaces (*arrows*). Intracellular fluorescent signals were also detected. The cellular localization of these mutants was indistinguishable from that of the wild-type Cx50. Nuclei were labeled with DAPI (*blue*). Phase-contrast images (*right*) show cell morphology. Scale bar, 20 μm.

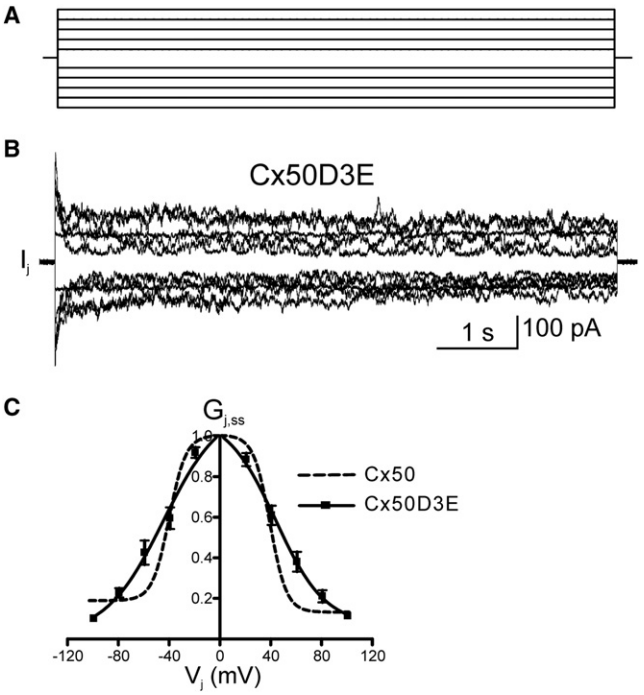


FIGURE 3 Macroscopic $V_j$-dependent gating properties of Cx50D3E gap junctions. (*A*) Voltage-step protocol (from ±20 to ±100 mV) applied to characterize $V_j$-dependent gating properties in N2A cell pairs. Only one cell of a pair underwent this protocol; the other cell was held at 0 mV. (*B*) A representative family of junctional currents recorded in N2A cell pair expressing Cx50D3E. (*C*) Normalized junctional conductance ($G_{j,ss}$, steady-state relative to maximal) is plotted as a function of $V_j$ and fit with Boltzmann equations ($n = 5$). Solid line, Boltzmann fitting curve; error bars, SE. The Boltzmann curve for Cx50 (15) is superimposed for comparison purposes (*dashed line*).

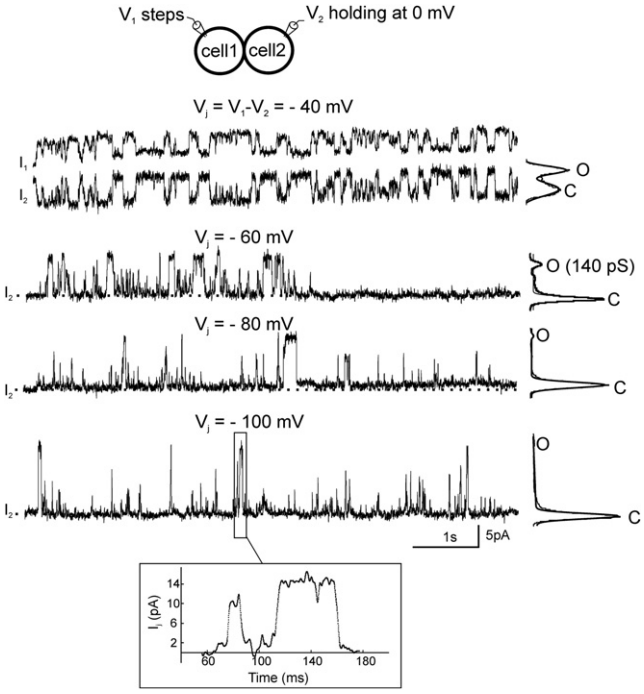


FIGURE 4 Single Cx50D3E gap junction channel activities. Representative single-channel currents recorded from cell 2 ($I_2$) in response to $V_j$ pulses of −40, −60, −80, and −100 mV applied to cell 1. The corresponding all-points amplitude histograms are shown to the right of each trace. The current recorded from cell 1 ($I_1$) at −40 mV is presented to show the symmetrical channel activities of $I_1$ and $I_2$. Transitions between open and closed states (*dashed line*) were detected at all $V_j$ pulses tested; however, the channel spent more time in the closed states with increasing $V_j$ steps. No long-lived substate was detected, although the channel frequently showed flickering transitions to incomplete-opening levels. (*Inset*) An expanded timescale (filtered at 1 kHz, with sampling intervals of 0.1 ms) shows a typical transition to/from incomplete opening and transitions between the fully open and closed states. The fully open state, $\gamma_j$, was 140 pS in this recording.

## Cx50D3E exhibits reduced unitary conductance

To assess the $V_j$-dependent transitions of a single Cx50D3E GJ channel, as well as to analyze the unitary conductance, junctional currents were measured in poorly coupled N2A cell pairs with one or two active channels. Representative single Cx50D3E GJ responses to $V_j$ pulses of −40, −60, −80, and −100 mV are illustrated in Fig. 4. At −40 mV, the channel displayed frequent transitions between the open and fully closed states. At more negative $V_j$ pulses, the dwell time in the open state is reduced. The mean dwell time of the main open state calculated from seven recordings at $V_j = \pm 40$ mV is 57 ± 11 ms (see Fig.7 *B*), which is significantly reduced from the dwell time for wild-type Cx50 (149 ± 7 ms; $p < 0.001$). It was also noted that although no evident long-lived substate was observed, the channel did show flickering (or brief) transitions to incomplete (multilevel) open states. A typical incomplete transition and a transition between the fully open and the closed state in the −100 mV trace are illustrated with an expanded timescale (Fig. 4, *inset*). Both types of transitions are slow, usually lasting tens of milliseconds. The fully open state, $\gamma_j$, derived from eight cell pairs was 139 ± 5 pS (mean ± SE), which is significantly lower than that of Cx50 (205 ± 5 pS; $p < 0.01$), as previously documented (15). These results demonstrate that the Cx50D3E substitution eliminates the substate observed in wild-type Cx50 GJ channels and reduces the $\gamma_j$ of the main open state. Moreover, the mean

**TABLE 1 Boltzmann parameters and Gibb's free energy**

| | $z$ | $V_0$ (mV) | $G_{min}$ | $\Delta G_0$ (kJmol$^{-1}$) | $V_j$ |
|---|---|---|---|---|---|
| Cx50 | 3.9 ± 1.0 | 38.4 ± 1.2 | 0.20 ± 0.01 | 14.6 ± 3.9 | − |
| | 4.0 ± 1.0 | 39.3 ± 1.0 | 0.15 ± 0.02 | 15.3 ± 4.0 | + |
| Cx50N9R | 2.3 ± 0.5 | 59.6 ± 2.7 | 0.04 ± 0.05 | 13.0 ± 3.1 | − |
| | 1.7 ± 0.3 | 57.8 ± 2.5 | 0.02 ± 0.05 | 9.4 ± 1.7 | + |
| Cx50G8E | 3.8 ± 0.6 | 30.8 ± 1.8 | 0.15 ± 0.02 | 11.1 ± 1.9 | − |
| | 4.0 ± 0.7 | 30.2 ± 1.8 | 0.15 ± 0.02 | 11.5 ± 2.1 | + |
| Cx50GNI | 4.1 ± 0.7 | 45.2 ± 1.3 | 0.17 ± 0.02 | 18.2 ± 3.2 | − |
| | 4.2 ± 0.8 | 46.2 ± 1.5 | 0.17 ± 0.02 | 18.8 ± 3.6 | + |
| Cx50D3E | 1.1 ± 0.4 | 45.1 ± 5.4 | 0.02 ± 0.01 | 4.9 ± 1.8 | − |
| | 1.3 ± 0.3 | 43.3 ± 3.9 | 0.07 ± 0.06 | 5.5 ± 1.4 | + |

Values for $V_0$ and $\Delta G_0$ are absolute values.

dwell time of the main open state at ±40 mV was significantly reduced.

### The $G_{j,ss}/V_j$ relationship of Cx50G8E and Cx50GNI gap junctions

To determine the $G_{j,ss}/V_j$ relationship of Cx50G8E and Cx50GNI gap junctions, the voltage steps described in Fig. 3 *A* were also conducted for these GJs. Families of representative macroscopic $I_j$ of Cx50G8E and Cx50GNI channels are shown in Fig. 5, *A* and *B*, respectively. The amplitude of the $I_j$ started to decline at lower $V_j$ steps for the Cx50G8E

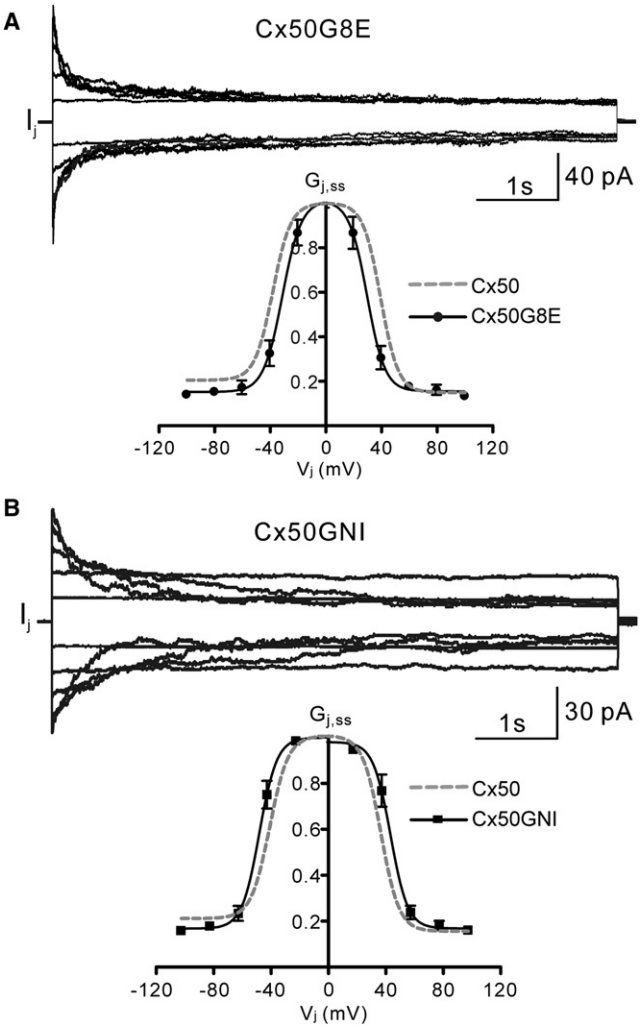


FIGURE 5 Macroscopic $V_j$-dependent gating properties of Cx50G8E and Cx50GNI gap junctions. (*A*) A family of $I_j$ recorded in one cell of a pair expressing Cx50G8E in response to the voltage steps applied to the other cell. $G_{j,ss}$ values are plotted against $V_j$ and fit with Boltzmann equations ($n = 4$; *solid line*, Boltzmann curve; error bars, SE). (*B*) A family of $I_j$ recorded in one cell of a pair expressing Cx50GNI in response to the voltage-steps applied to the other cell. $G_{j,ss}$ are plotted against $V_j$ and fit with Boltzmann equations ($n = 6$; *solid line*, Boltzmann fitting curve; error bars, SE). The Boltzmann fitting curve for Cx50 (15) is superimposed for comparison purposes (*gray dashed line*).

(±20 mV) than for the Cx50GNI channel (±40 mV). The steady-state $G_j$ values were normalized to their corresponding peak $G_j$, plotted against $V_j$, and fit with Boltzmann equations (Fig. 5, *A* and *B*). As compared to wild-type Cx50, both mutants shifted the $V_0$ by ~8 mV (inward shifts for G8E and outward for GNI) without changing the apparent gating-charge valence. The Cx50G8E channels produced $\Delta G_0$ values of 11.1 ± 1.9 and 11.5 ± 2.1 kJ mol$^{-1}$ for negative and positive $V_j$, respectively. The Cx50GNI channels produced corresponding $\Delta G_0$ values of 18.2 ± 3.2 and 18.8 ± 3.6 kJ mol$^{-1}$. No significant difference in $\Delta G_0$ was found ($p > 0.05$) for either mutant channel relative to the wild-type, but there is a significant difference between these two mutants for both $V_j$ polarities ($p < 0.01$). Mean values for the Boltzmann parameters and $\Delta G_0$ are given in Table 1. These results demonstrate that G8E substitution and GNI triple mutation affect neither the $V_j$-dependent gating sensitivity nor the stability of the channel between the open and closed states relative to the wild-type. Nonetheless, as compared to G8E, the GNI triple mutation increased the energy difference between the open and closed states. This had the effect of favoring the open state at all voltages.

The $V_j$-dependent gating kinetics of G8E, GNI, and D3E mutant GJ channels were analyzed and the results are presented in the Supporting Material. Neither D3E nor G8E substitutions affected the time constant of macroscopic junctional current relaxation at any of the tested $V_j$ pulses, whereas GNI substitution significantly prolonged the time constant at $V_j = \pm 100$ mV (Fig. S1).

### Cx50G8E and Cx50GNI mutants retain substate and unchanged unitary conductance

We performed double whole-cell patch-clamp recordings in poorly coupled N2A pair cells transfected with Cx50G8E or Cx50GNI. Representative single-channel recordings under different $V_j$ steps are shown in Fig. 6, *A* and *B*. In contrast to the D3E substitution, both G8E and GNI mutants exhibited an obvious long-lived substate, which is reminiscent of wild-type Cx50 GJ channels reported in our previous study (15). Transitions between the fully open state and the substate were observed at all $V_j$ pulses tested, and the substate occupancy was increasing with higher $V_j$ pulses (see all-points amplitude histograms in Fig. 6, *A* and *B*). Fig. 6 *C* shows the averaged $\gamma_j$ of Cx50G8E (open state, 222 ± 4 pS; substate, 42 ± 3 pS; $n = 6$ cell pairs), Cx50GNI (open state, 216 ± 6 pS; substate, 42 ± 2 pS; n = 6 cell pairs), and Cx50 (open state, 205 ± 5 pS; substate, 39 ± 4 pS; n = 11 cell pairs). There was no significant difference in unitary conductance among either the main open states or the substates of these channels (Fig. 6 *C*; $p > 0.05$). The analysis from seven cell pairs expressing single Cx50G8E channels yields a mean dwell time of the main open state at ±40 mV of 142 ± 11 ms, which is not significantly different from that of wild-type Cx50

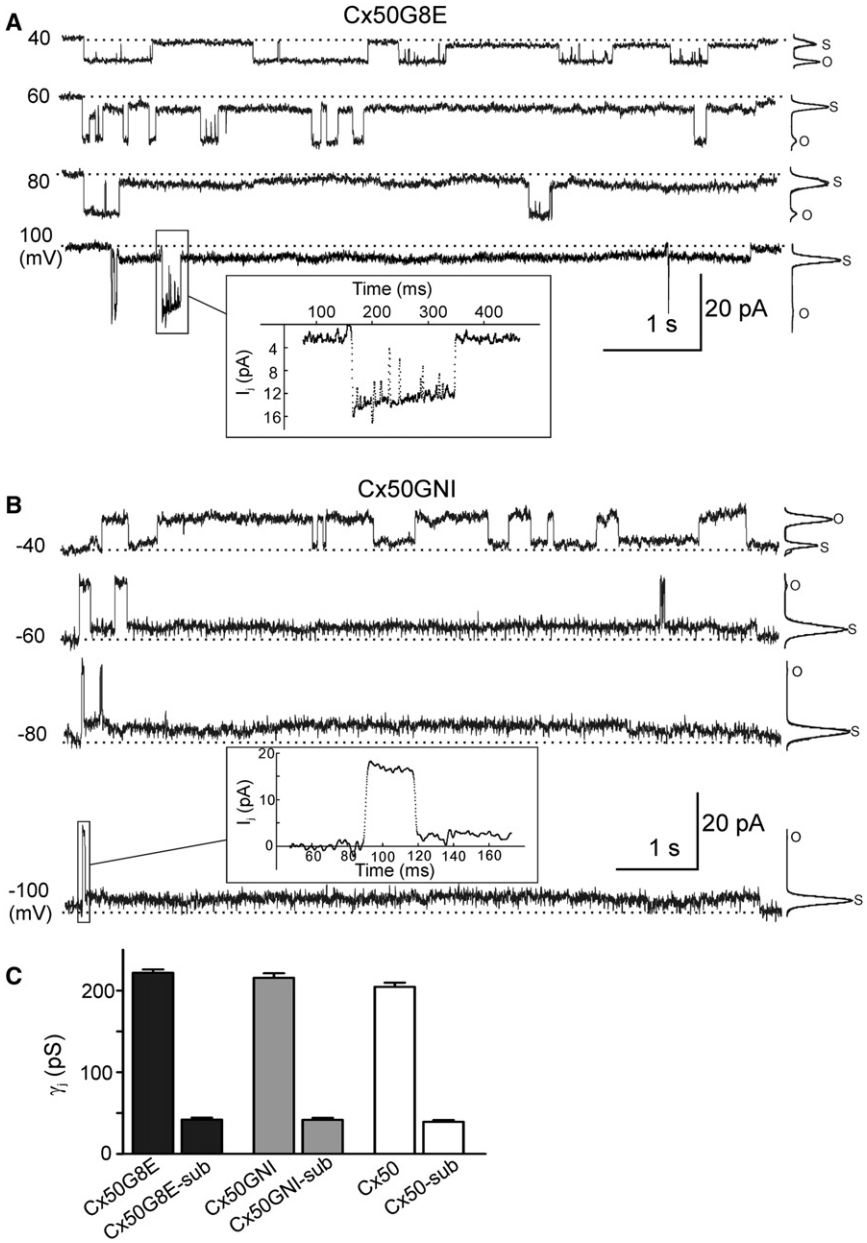


FIGURE 6 Cx50G8E and Cx50GNI channels showed similar single-channel conductance to the Cx50 GJ channel. Cx50G8E (*A*) and Cx50GNI (*B*) single GJ channel currents recorded from N2A cell pairs. Main open state, substate, and closed state (*dashed lines*) were observed in these two mutant GJ channels. (*Insets*) Expanded timescales (filtered at 1 kHz, with sampling intervals of 0.1 ms) show typical fast transitions between the open state and substates. Both mutant channels spent more time in the substate with increasing $V_j$ steps. (*C*) Neither the main open state nor the substate $\gamma_j$ of Cx50G8E and Cx50GNI showed significant differences from those of the Cx50 GJ channel.

($p > 0.05$ (Fig. 7)). However, the Cx50GNI single-channel recordings sampled from five recordings at $\pm 40$ mV yielded a significantly longer mean dwell time of the main open state (488 $\pm$ 8 ms; $p < 0.001$ (Fig. 7)). From these results, we conclude that G8E and GNI mutants retain the substate observed in the wild-type and fail to alter the unitary conductance of the main open state and substate. However, GNI substitution significantly prolonged the dwell time of the main open state at $\pm 40$ mV.

## DISCUSSION

In this study, we examined the $V_j$-dependent gating properties of three mutants (Cx50D3E, Cx50G8E, and Cx50GNI) expressed in N2A cells, both macroscopically and at the single-channel level. Our key objective was to evaluate whether the D3 residue in Cx50 plays a role, in addition to that of providing a negative charge, in determining the polarity of $V_j$-dependent gating. Our strategy was to substitute another negatively charged residue (the D3E substitution) and comprehensively assess changes in channel function. In addition, the examination of this mutant may also assist our understanding of the role of the E residue in determining the $V_j$-gating properties of other Cxs, such as Cx36 and hCx31.9. Our key finding was that the D3E substitution caused $V_j$-dependent changes both macroscopically and at the single-channel level. Macroscopically, a minor shift in $V_0$ could be accounted for by the reduced

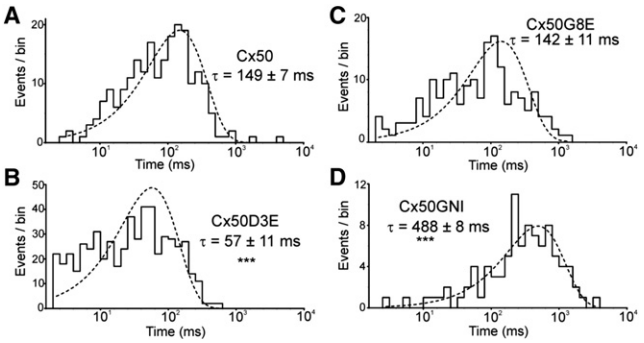


FIGURE 7 Open-dwell-time histograms. The logarithmic histograms (10 bins/decade) of the dwell time of the main open state at $V_j = \pm 40$ mV are illustrated. Data from +40 mV are similar to those of −40 mV and they are pooled together. All histograms are fit with one exponential (*dotted lines*) with their mean dwell time indicated on the graphs. ***Statistically significant difference ($p < 0.001$) from wild-type Cx50.

gating-charge valence and reduced $\Delta G_0$ between the aggregate open and closed states. Single Cx50D3E GJ channels failed to show a long-lived substate, and the $\gamma_j$ of the main open state was reduced by ~30%. By contrast, G8E and GNI substitutions did not alter the $V_j$-dependent gating sensitivity; single GJ channels retained a long-lived substate and unchanged unitary conductance.

## Effects of the D3E mutation in Cx50

Since Verselis and colleagues reported the important role of the second residues of Cx26 (Asp-2) and Cx32 (Asn-2) in determining the polarity of fast $V_j$-gating (12), mutational studies on other Cxs, such as Cx50 and Cx46 (14), have been conducted to elucidate the role of the equivalent residue (D3) in determining their $V_j$-gating profiles. Neutralization of the D3 residues of Cx50 and Cx46 by an Asn residue in an effort to selectively affect the polarity of fast $V_j$-gating was unexpectedly found to show effects on $V_j$-dependent gating behaviors in addition to the reversal of their gating polarity. These studies suggest involvement of the negatively charged D3 residue in $V_j$-sensing, so a D-to-E substitution is not expected to have an effect on $V_j$-sensing beyond that of simply providing a negative charge. We discuss here how the D3E substitution in Cx50 in N2A cells not only alters the $V_j$-gating phenotype, and these properties also hold many similarities with the D3N substitution studied in *Xenopus* oocytes (14). For example, the macroscopic $G_j$ of D3N GJ channels exhibited near-zero residual conductance at high $V_j$s, and the Boltzmann fitting of the $G_{j,ss}/V_j$ relation in our study in D3E GJ channels similarly produced a near-zero $G_{min}$. In addition, a single D3N hemichannel showed reduced $\gamma_j$ (by 70%), lack of substate, and frequent incomplete opening transitions; in a similar way, our single D3E GJ channel displayed reduced $\gamma_j$ (by 30%), and no long-lived substate was detected, although incompletely opening transitions occurred frequently. These similarities suggest that D3N and D3E substitutions may induce a similar modification in Cx50 channel conformation, indicating a specific and unique role of the D3 residue in determining Cx50 channel pore properties. Despite these similarities, a definitive conclusion cannot be drawn by virtue of the fact that these two studies were performed in different cells and the single-channel data were compared between hemichannels in D3N and whole GJ channels in D3E.

The Boltzmann fit of the $G_{j,ss}/V_j$ relation allows us to detect the effect of D3E substitution on the $V_j$-dependent gating process. The proposed voltage-gating model for voltage-gated ion channels is that during the gating process, a change in the voltage results in a reorientation of dipoles or movement of charge relative to the field. A voltage sensor produces a conformational change of the channel that leads to closing or opening the channel (26). Boltzmann fit of the $G_{j,ss}/V_j$ relation assumes that gap junction channels make transitions between two states (open and closed) and that the energy difference between these states is linearly related to $V_j$ (3,21). The change in $V_0$ is a function of changes in gating charge and free energy difference between the open and closed states. The D3E substitution caused a minor change in $V_0$, which can be accounted for by both a reduced apparent gating charge, $z$ (by ~70%), and a reduced free-energy difference between the open and closed states (by ~70%). The value of $z$ is a function of the total displacement of charge in the potential field, so a lower $z$ could arise from either fewer charges in the voltage sensor or less displacement of the voltage sensor through the voltage field (27). The D3E substitution does not involve a change in the charge of the residue, so the reduced gating-charge valence may occur because this mutation restricts the movement of the voltage sensor through the voltage field.

The reduced $\Delta G_0$ between the open and closed states caused by D3E substitution reflects a shift of the equilibrium between the two states at $V_j = 0$. This could be caused by stabilization of the closed state, destabilization of the open state, or both. At the single-channel level, the reduced open dwell time at $\pm 40$ mV indicates a destabilization of the open state. However, the stability of the closed state was not measured due to the existence of both substates and fully closed states. Wild-type Cx50 GJ channels show a long-lasting substate, as well as short and occasionally full closures, whereas the D3E GJ channel only shows full closures. Thus, it would be problematic to compare the substate of wild-type with the closed state of the D3E mutant GJ channel. A previous study on the Kv1 potassium channel (27) indicates that an additional methylene group in the side chain of the E residue leads to significant stabilization of the open state, given the fact that N227E, but not N227D, substitution shifted the channel equilibrium strongly toward the open state. Thus, it appears to be reasonable to suggest that the D3 residue in Cx50 critically determines the open-closed stability. Nonetheless, without an

atomic structure of the Cx50 GJ in the open and/or closed conformations, as well as further mutational studies, the underlying mechanisms of the effect of D3E on the open-closed stability cannot be resolved.

The $\gamma_j$ of Cx50D3E GJ was reduced by ~30%, and this may be partially, if not entirely, due to the steric effect imposed by the longer side chain of the E residue. Whether or not an electrostatic effect on $\gamma_j$ is involved remains elusive in the absence of detailed structural information. For example, if D3E substitution induces a conformational change, other residues initially buried in the membrane lipid could be exposed to the conductive pathway, which in turn would alter the $\gamma_j$ of the channel. In addition, the long-lived substate observed in the wild-type Cx50 channel was absent in the Cx50D3E GJ channel. Instead, apparent transitions between the open and the fully closed states were accompanied by flickering transitions to the incomplete open state. These transitions typically took tens of milliseconds. It has been suggested that GJs have two $V_j$-gating mechanisms, fast $V_j$-gating and slow $V_j$-gating, based on the time course of gating transitions between different states. The fast $V_j$-gating was suggested to be responsible for the transitions between open state and substate, whereas the slow $V_j$-gating mechanism underlies transitions to the fully closed state (28). Based on the above $V_j$-gating mechanism, one possible explanation for the lack of substate is that in the mutant, slow $V_j$-gating may predominate throughout the range of voltages examined; alternatively, the fast $V_j$-gating mechanism may be impaired. However, at present, we are not able to determine whether the D3E substitution alters the fast $V_j$-gating mechanism. Study of heterotypic GJ channels formed by Cx50D3E and another type of connexin with known $V_j$-dependent gating polarity (e.g., the fast gate for wild-type Cx50 was suggested to have positive polarity), or of Cx50D3E hemichannels, would help address this issue.

In an attempt to elucidate the role of the E3 residue in Cx36, we tested a Cx36E3D mutant but failed to detect any functional GJ channels (L. Xin and D. Bai, unpublished observations). This may be due to the limitations of our system; at any rate, the current data do not permit us to draw any definitive conclusion regarding the role of the E3 residue in Cx36 $V_j$-dependent gating properties.

### Effects of G8E and GNI mutations in Cx50

The voltage-sensing region of gap junction channels was suggested to be lining the aqueous pore (4) rather than residing in a separate domain, as is the case for voltage-dependent potassium channels (29). Both structural and functional studies have suggested that part of the NT of connexins lines the channel pore, and charged residues in the NT may determine key aspects of $V_j$-gating, $\gamma_j$, and charge selectivity of ion permeation (18,26,30–34). According to a recently documented hCx26 crystal structure, the NT folds into the mouth of the channel and forms a funnel structure to constrict the cytoplasmic entrance of the pore (35). The funnel surface of hCx26 was lined by residues Asp-2, Trp-3, Thr-5, Leu-6, and Ile-9. The Asp-2 from the six Cx26 subunits forms the narrowest part of the channel. This raises the possibility that the equivalent residue (i.e., E) residing at different positions in the NT may influence channel pore properties (e.g., $V_j$-gating and $\gamma_j$) in a different manner. In light of this notion, we tested the effect of an E residue in the eighth position (G8E mutation) of the NT on Cx50 GJ channel properties.

In contrast to the effects of D3E, the G8E substitution did not affect the $V_j$-dependent gating sensitivity, as reflected by the unchanged gating-charge valence, nor was the relative stability between the open and closed states affected. Previously, we documented a reduced $\gamma_j$ for N9R substitution; one may expect an increased $\gamma_j$ for G8E substitution, since substitution of the oppositely charged residue at the next position (N9R) decreases $\gamma_j$. However, the $\gamma_j$ of G8E channels presented here is indistinguishable from Cx50. This suggests that G8E substitution does not effectively impose steric and electrostatic constraints on ion permeation. This suggestion is supported by the Cx26 crystal structure, which shows that the eighth position of the NT is close to the intracellular wide opening part of the channel. In addition, previous study (36) has suggested that Cx50 channels are selective for cations over anions; thus, if the cations accumulated at the channel intracellular entrance are already saturated, addition of a negatively charged residue nearby would not recruit more cations. At present, we cannot rule out other possibilities in the absence of detailed structural information and ion replacement experiments. Nevertheless, these findings imply a more critical role in determining these properties for the third-position than the eighth-position residue of Cx50 NT.

Sequence alignment of Cx36 and Cx50 NTs shows several amino acid differences. To identify critical residues in the NT, we generated a triple mutant that changed three amino acids in the middle section of the NT to match those of Cx36 (GNI mutant; G8E + N9R + I10L). We were surprised to find that this triple mutant did not alter the $V_j$-gating sensitivity or the free-energy difference between the open and closed states. One possible explanation for the unchanged Boltzmann parameters is that the negatively charged E8 may offset the effect of residue R9 on channel properties by electrostatic interactions. However, we cannot prove or rule out a potential role of I10L substitution without testing the effect of the double mutant G8E + N9R. The GNI mutant did not change the free-energy difference between the aggregate open and closed states, but we observed an increased mean open dwell time at $\pm 40$ mV, indicating an increased transition barrier going from the open to the closed state. This argument is further supported by the slower relaxation of macroscopic junctional currents at $\pm 100$ mV (see the Supporting Material). Nevertheless,

conclusions drawn from this observation should be made with caution. The first-order kinetics observed by Harris et al. (4) does not apply to this case, which therefore complicates the analysis of the gating kinetics of the Cx50GNI channels.

In summary, a previous study demonstrated a role for the D3 residue in determining the polarity of $V_j$-dependent gating. This study reveals additional roles of D3 in determining Cx50 GJ properties. However, as to the role played by the aspartic acid residue at the second or third position of other Cxs (e.g., Cx30, Cx37, Cx40, Cx46, and Cx43) in their $V_j$-gating and unitary conductance remains to be determined. Thus, further investigation is required to differentiate the role of the glutamic acid residue (third position) in Cx36, hCx31.9, or mCx30.2 GJ channel properties from that of the aspartic acid residue (third position) in Cx50.

## SUPPORTING MATERIAL

Results, two references, and a figure are available at http://www.biophysj.org/biophysj/supplemental/S0006-3495(12)00208-1.

We thank Drs. Feng Qin and Jie Zheng for their helpful discussions on single-channel analysis and Yuhua Dong for technical help.

This work was supported by a grant to D.B. from the Natural Sciences and Engineering Research Council of Canada. D.B. is also supported by the Canadian Institutes of Health Research and an Early Researcher Award from the Ontario government. This work was also supported by a Grant-in-Aid fellowship for the Japan Society for the Promotion of Science, the Global Center of Excellence program Global Education and Research Center for Bio-Environmental Chemistry of Osaka University, the Institutional Program for Young Researcher Overseas Visits (to S.N.), and Grants-in-Aid for Scientific Research (16087206, 18207006, and 21227003) from the Ministry of Education, Culture, Sports, Science and Technology of Japan (to T.T.).

## REFERENCES

1. Harris, A. L. 2001. Emerging issues of connexin channels: biophysics fills the gap. *Q. Rev. Biophys.* 34:325–472.
2. González, D., J. M. Gómez-Hernández, and L. C. Barrio. 2007. Molecular basis of voltage dependence of connexin channels: an integrative appraisal. *Prog. Biophys. Mol. Biol.* 94:66–106.
3. Spray, D. C., A. L. Harris, and M. V. Bennett. 1981. Gap junctional conductance is a simple and sensitive function of intracellular pH. *Science.* 211:712–715.
4. Harris, A. L., D. C. Spray, and M. V. Bennett. 1981. Kinetic properties of a voltage-dependent junctional conductance. *J. Gen. Physiol.* 77: 95–117.
5. Steiner, E., and L. Ebihara. 1996. Functional characterization of canine connexin45. *J. Membr. Biol.* 150:153–161.
6. Teubner, B., J. Degen, …, K. Willecke. 2000. Functional expression of the murine connexin 36 gene coding for a neuron-specific gap junctional protein. *J. Membr. Biol.* 176:249–262.
7. Jiang, J. X., T. W. White, …, D. L. Paul. 1994. Molecular cloning and functional characterization of chick lens fiber connexin 45.6. *Mol. Biol. Cell.* 5:363–373.
8. White, T. W., R. Bruzzone, …, D. A. Goodenough. 1994. Selective interactions among the multiple connexin proteins expressed in the vertebrate lens: the second extracellular domain is a determinant of compatibility between connexins. *J. Cell Biol.* 125:879–892.
9. Al-Ubaidi, M. R., T. W. White, …, R. Bruzzone. 2000. Functional properties, developmental regulation, and chromosomal localization of murine connexin36, a gap-junctional protein expressed preferentially in retina and brain. *J. Neurosci. Res.* 59:813–826.
10. White, T. W., M. Srinivas, …, R. Bruzzone. 2002. Virtual cloning, functional expression, and gating analysis of human connexin31.9. *Am. J. Physiol. Cell Physiol.* 283:C960–C970.
11. Kreuzberg, M. M., G. Söhl, …, F. F. Bukauskas. 2005. Functional properties of mouse connexin30.2 expressed in the conduction system of the heart. *Circ. Res.* 96:1169–1177.
12. Verselis, V. K., C. S. Ginter, and T. A. Bargiello. 1994. Opposite voltage gating polarities of two closely related connexins. *Nature.* 368:348–351.
13. Peracchia, C., and L. L. Peracchia. 2005. Inversion of both gating polarity and $CO_2$ sensitivity of voltage gating with D3N mutation of Cx50. *Am. J. Physiol. Cell Physiol.* 288:C1381–C1389.
14. Srinivas, M., J. Kronengold, …, V. K. Verselis. 2005. Correlative studies of gating in Cx46 and Cx50 hemichannels and gap junction channels. *Biophys. J.* 88:1725–1739.
15. Xin, L., X. Q. Gong, and D. Bai. 2010. The role of amino terminus of mouse Cx50 in determining transjunctional voltage-dependent gating and unitary conductance. *Biophys. J.* 99:2077–2086.
16. Gong, X. Q., Q. Shao, …, D. W. Laird. 2007. Differential potency of dominant negative connexin43 mutants in oculodentodigital dysplasia. *J. Biol. Chem.* 282:19190–19202.
17. Srinivas, M., R. Rozental, …, D. C. Spray. 1999. Functional properties of channels formed by the neuronal gap junction protein connexin36. *J. Neurosci.* 19:9848–9855.
18. Musa, H., E. Fenn, …, R. D. Veenstra. 2004. Amino terminal glutamate residues confer spermine sensitivity and affect voltage gating and channel conductance of rat connexin40 gap junctions. *J. Physiol.* 557:863–878.
19. Moreno, A. P., B. Eghbali, and D. C. Spray. 1991. Connexin32 gap junction channels in stably transfected cells. Equilibrium and kinetic properties. *Biophys. J.* 60:1267–1277.
20. Wilders, R., and H. J. Jongsma. 1992. Limitations of the dual voltage clamp method in assaying conductance and kinetics of gap junction channels. *Biophys. J.* 63:942–953.
21. Rubin, J. B., V. K. Verselis, …, T. A. Bargiello. 1992. A domain substitution procedure and its use to analyze voltage dependence of homotypic gap junctions formed by connexins 26 and 32. *Proc. Natl. Acad. Sci. USA.* 89:3820–3824.
22. Bai, D., C. del Corsso, …, D. C. Spray. 2006. Block of specific gap junction channel subtypes by 2-aminoethoxydiphenyl borate (2-APB). *J. Pharmacol. Exp. Ther.* 319:1452–1458.
23. Sigworth, F. J., and S. M. Sine. 1987. Data transformations for improved display and fitting of single-channel dwell time histograms. *Biophys. J.* 52:1047–1054.
24. Yifrach, O., and R. MacKinnon. 2002. Energetics of pore opening in a voltage-gated $K^+$ channel. *Cell.* 111:231–239.
25. Sukhareva, M., D. H. Hackos, and K. J. Swartz. 2003. Constitutive activation of the Shaker $K_v$ channel. *J. Gen. Physiol.* 122:541–556.
26. Bezanilla, F. 2000. The voltage sensor in voltage-dependent ion channels. *Physiol. Rev.* 80:555–592.
27. Klassen, T. L., M. L. O'Mara, …, W. J. Gallin. 2008. Non-linear intramolecular interactions and voltage sensitivity of a $K_V1$ family potassium channel from *Polyorchis penicillatus* (Eschscholtz 1829). *J. Exp. Biol.* 211:3442–3453.
28. Bukauskas, F. F., C. Elfgang, …, R. Weingart. 1995. Biophysical properties of gap junction channels formed by mouse connexin40 in induced pairs of transfected human HeLa cells. *Biophys. J.* 68:2289–2298.

29. Long, S. B., E. B. Campbell, and R. Mackinnon. 2005. Crystal structure of a mammalian voltage-dependent *Shaker* family $K^+$ channel. *Science.* 309:897–903.

30. Oh, S., V. K. Verselis, and T. A. Bargiello. 2008. Charges dispersed over the permeation pathway determine the charge selectivity and conductance of a Cx32 chimeric hemichannel. *J. Physiol.* 586:2445–2461.

31. Purnick, P. E., S. Oh, …, T. A. Bargiello. 2000. Reversal of the gating polarity of gap junctions by negative charge substitutions in the N-terminus of connexin 32. *Biophys. J.* 79:2403–2415.

32. Dong, L., X. Liu, …, L. Ebihara. 2006. Role of the N-terminus in permeability of chicken connexin45.6 gap junctional channels. *J. Physiol.* 576:787–799.

33. Tong, J. J., X. Liu, …, L. Ebihara. 2004. Exchange of gating properties between rat cx46 and chicken cx45.6. *Biophys. J.* 87:2397–2406.

34. Tong, J. J., and L. Ebihara. 2006. Structural determinants for the differences in voltage gating of chicken Cx56 and Cx45.6 gap-junctional hemichannels. *Biophys. J.* 91:2142–2154.

35. Maeda, S., S. Nakagawa, …, T. Tsukihara. 2009. Structure of the connexin 26 gap junction channel at 3.5 Å resolution. *Nature.* 458:597–602.

36. Srinivas, M., M. Costa, …, D. C. Spray. 1999. Voltage dependence of macroscopic and unitary currents of gap junction channels formed by mouse connexin50 expressed in rat neuroblastoma cells. *J. Physiol.* 517:673–689.